On the inadvisability of using single parameter impedance models for representing the acoustical properties of ground surfaces

Didier Dragna[a)]
Laboratoire de Mécanique des Fluides et d'Acoustique, Unité Mixte de Recherche 5509, Centre National de la Recherche Scientifique, École Centrale de Lyon, Université de Lyon, 36, Avenue Guy de Collongue, 69134 Écully Cedex, France

Keith Attenborough
Engineering and Innovation, The Open University, Milton Keynes, MK7 6AA, United Kingdom

Philippe Blanc-Benon
Laboratoire de Mécanique des Fluides et d'Acoustique, Unité Mixte de Recherche 5509, Centre National de la Recherche Scientifique, École Centrale de Lyon, Université de Lyon, 36, Avenue Guy de Collongue, 69134 Écully Cedex, France

(Received 23 June 2015; revised 26 August 2015; accepted 9 September 2015; published online 23 October 2015)

Although semi-empirical one parameter models are used widely for representing outdoor ground impedance, they are not physically admissible. Even when corrected to satisfy a passivity condition in respect of surface impedance they do not satisfy the condition that the real part of complex density must be greater than zero. Comparison of predictions with frequency-domain data for short range propagation have indicated that physically admissible models provide superior overall agreement. A two parameter variable porosity model yields better agreement for many grassland surfaces and a two parameter version of the slit pore microstructural impedance model yields better agreement with data obtained over low flow resistivity surfaces such as forest floors and gravel. Impedance models and conditions for physical admissibility are summarised. In addition to those examined previously, the slit pore model is shown to be physically admissible. After providing further examples of the better agreement with short range data that can be achieved using two parameter models, it is shown that differences between frequency domain predictions at longer ranges using physically admissible models rather than one parameter models are significantly greater than those resulting from short range spatial variability and comparable with seasonal variability over grassland. © *2015 Acoustical Society of America.*
[http://dx.doi.org/10.1121/1.4931447]

[DKW] Pages: 2399–2413

I. INTRODUCTION

When predicting outdoor sound at long range including effects of discontinuous ground, meteorology, diffraction by natural and artificial barriers, and topography, it is tempting to use the simplest possible descriptions of the acoustical properties of porous ground surfaces. Consequently, single-parameter semi-empirical models for the acoustical properties of (rigid-framed) porous materials due to Delany and Bazley[1] and Miki[2] are widely used. The Delany and Bazley model has been used in this way since the 1970s and use of the Miki model, which was introduced to overcome non-physical predictions of the Delany and Bazley model, in calculations related to outdoor sound has become increasingly popular in the last decade.

Standard methods for determining ground impedance spectra [ANSI S1.18 2010,[3] NTACOU 104 (Ref. 4)] include the option of choosing parameter values for the Delany and Bazley model that, when used with the classical theory for propagation from a point source over an impedance plane, enable best fit to measurements of spectra of the magnitude of the difference in levels recorded by vertically separated microphones at a short range from an omnidirectional source. The Delany and Bazley model is also recommended as one of the default impedance models in the HARMONOISE engineering model,[5] and is likely to feature as a default ground impedance model when making the predictions required for noise mapping in response to the European Noise Directive.[6]

There are many models for the acoustical properties of rigid-framed porous materials, 14 of which were reviewed for representing ground surface impedance elsewhere.[7] The more sophisticated models require knowledge of some parameter values that are not available routinely for outdoor ground surfaces and their evaluation from short range propagation data would be problematic. After using the relationship between tortuosity and porosity for stacked spheres, a shortlist of five models that need no more than two adjustable parameters and which could be used as convenient alternatives for representing the impedance of porous outdoor ground surfaces, have been investigated further.[7] With the

a)Electronic mail: didier.dragna@ec-lyon.fr

same input parameter values, three models, namely, those of Wilson,[8] Hamet,[9] and a model that assumes a microstructure of slit like pores,[7] give more or less identical predictions of surface impedance spectra. As will be considered later, the slit pore model requires calculations of hyperbolic tangent functions. However, these are required anyway when calculating the impedance of a hard-backed layer. Consequently the slit pore model is considered further here. After comparing predictions using four of the short-listed impedance models with short range level difference magnitude data, it has been shown that a two-parameter variable porosity impedance model yields better fits than either single-parameter (semi-infinite) or two-parameter (hard-backed layer) empirical models for grassland and that a two-parameter version of the slit pore microstructural model leads to better fits than the empirical models for low flow resistivity surfaces such as forest floors and gravel.[7] With respect to time-domain predictions of outdoor sound propagation, it has been shown that the empirical single parameter models and hard-backed layer versions of them do not meet the requirements for physical admissibility.[10]

After reviewing the conditions for physical admissibility, Sec. II of this paper extends the analysis in Ref. 10 to show that (a), even when modified to avoid predictions of negative real parts of surface impedance, the Miki model[2] can predict negative values of the real part of complex density and that (b) slit pore microstructural models for the impedance of semi-infinite and hard-backed layers are physically admissible.

Section III extends previously published fitting of short range propagation data[7] to include two formulations of the Miki model.[2,11] Section IV demonstrates that significant differences in longer range predictions in both time- and frequency-domains result from using physically admissible (and better short range fitting) impedance models rather than physically inadmissible empirical impedance models. Moreover it is pointed out that more or less identical fits to measurements of level difference magnitude spectra such as involved in standards for measuring ground impedance can be obtained with impedance spectra that differ significantly, particularly at the lower frequencies. The resulting differences in predictions of longer range propagation are compared with those predicted from measured spatial and seasonal variations[12] at two grass-covered sites. Section V offers concluding remarks.

II. PHYSICALLY ADMISSIBLE IMPEDANCE MODELS

A. Conditions for physically admissibility

Impedance models are classically defined in the frequency domain as the large majority of studies have been performed in the frequency domain. During the past 15 years, time-domain methods are becoming increasingly popular in the outdoor sound propagation community. However, some crucial issues for time-domain prediction, such as causality, were not thoroughly studied. Following Rienstra,[13] three conditions for the physical admissibility of surface impedance models were proposed in Ref. 10. First, the surface impedance model has to satisfy the reality condition

$$\text{Condition 1}: \quad \overline{Z_S}(\omega) = Z_S(-\omega),$$

where ω is the angular frequency related to the frequency f by $\omega = 2\pi f$ and the overbar denotes the complex conjugate. This condition guarantees that for a real-valued excitation, the acoustic variables are real-valued. Second, it has to verify the passivity condition

$$\text{Condition 2}: \quad \mathrm{Re}[Z_S(\omega)] \geq 0, \quad \text{for}\, \omega > 0,$$

which ensures that the ground absorbs acoustic energy and does not produce it. Third, it has to be causal, which can be checked using the causality condition 3,

$$\text{Condition 3.a}: \quad Z_S(\omega)\ \text{is analytic in}\ \mathrm{Im}(\omega) \geq 0,$$

$$\text{Condition 3.b}: \quad |Z_S(\omega)|\ \text{is square integrable over the real}\ \omega\text{–axis},$$

$$\text{Condition 3.c}: \quad \text{there is a real}\ t_0\ \text{such that}\ Z_S(\omega)e^{-i\omega t_0} \rightarrow 0\ \text{uniformly with regard to}\ \mathrm{Arg}(\omega)\ \text{for}\ |\omega| \rightarrow \infty\ \text{in}\ \mathrm{Im}(\omega) \geq 0.$$

These three conditions were investigated for two types of surface impedances, being a semi-infinite ground with surface impedance

$$Z_{S,\infty} = Z_c, \tag{1}$$

where Z_c is the characteristic impedance of the equivalent fluid and a rigidly backed layer, with surface impedance

$$Z_{S,d} = Z_c \coth(-ik_c d), \tag{2}$$

with d the thickness of the layer and k_c the propagation constant and for two families of impedance models. The first family, called the square-root type impedance model, includes phenomenological (see, e.g., Ref. 14) and Hamet[9] models, which have the general form

$$Z_c = \frac{\rho_0 c_0 \sqrt{T}}{\Omega} \alpha \left[\frac{(\omega_1 - i\omega)(\omega_2 - i\omega)}{-i\omega(\omega_3 - i\omega)} \right]^{1/2}, \tag{3a}$$

$$k_c = \frac{\omega \sqrt{T}}{c_0} \beta \left[\frac{(\omega_1 - i\omega)(\omega_3 - i\omega)}{-i\omega(\omega_2 - i\omega)} \right]^{1/2}, \tag{3b}$$

where ρ_0 is the air density, c_0 the sound speed in air, T and Ω are the tortuosity and the porosity of the porous medium, respectively, and α, β, ω_1, ω_2, and ω_3 are positive coefficients which depend on the characteristics of the porous medium. A closely related model is the variable porosity model, which corresponds to a low frequency/high flow resistivity approximation for the surface impedance of a rigid-porous medium in which the porosity decreases exponentially with depth at a rate α_e/m,[7]

$$Z_S = \rho_0 c_0 \left(\sqrt{\frac{4\sigma}{-i\omega\gamma\rho_0}} + \frac{c_0 \alpha_e}{-i\omega 4\gamma} \right), \tag{4}$$

TABLE I. Coefficients of the polynomial models in Eqs. (5), computed using an air density $\rho_0 = 1.2\,\mathrm{kg\,m^{-3}}$.

<table>
<tr><th></th><th>a</th><th>c</th><th>b</th><th>d</th><th>p</th><th>r</th><th>q</th><th>s</th></tr>
<tr><td>Delany and Bazley (Ref. 1)</td><td>0.232</td><td>0.336</td><td>0.75</td><td>0.73</td><td>0.353</td><td>0.576</td><td>0.70</td><td>0.59</td></tr>
<tr><td>Miki (Ref. 2)</td><td>0.251</td><td>0.384</td><td colspan="2">0.632</td><td>0.380</td><td>0.557</td><td colspan="2">0.618</td></tr>
<tr><td>Modified Miki (Ref. 10)</td><td>0.251</td><td>0.384</td><td colspan="2">0.632</td><td>0.351</td><td>0.539</td><td colspan="2">0.632</td></tr>
</table>

where σ is the air flow resistivity of the medium and γ is the ratio of specific heats in air. Equation (4) has the same form as a low frequency/high flow resistivity approximation of the impedance of a thin non-hard-backed layer of thickness $4/\alpha_e$.[7]

The second family is composed of polynomial models

$$Z_c = \rho_0 c_0 \left[1 + a\left(\frac{\sigma}{\rho_0\omega}\right)^b + ic\left(\frac{\sigma}{\rho_0\omega}\right)^d \right], \tag{5a}$$

$$k_c = \frac{\omega}{c_0} \left[1 + p\left(\frac{\sigma}{\rho_0\omega}\right)^q + ir\left(\frac{\sigma}{\rho_0\omega}\right)^s \right], \tag{5b}$$

where a, b, c, d, p, q, r, and s are constant coefficients. The most well-known polynomial models are the Delany and Bazley[1] and Miki[2] models, whose coefficients have been deduced from fitting a large body of impedance tube data for fibrous materials. The coefficients of these models are given in Table I. After comparing his original model with low frequency/high flow resistivity forms of the identical capillary pore model for rigid porous media, Miki proposed a three-parameter form of his model[11] in which the right-hand side of Eq. (5a) is multiplied by $\sqrt{T}/\Omega$ and that of Eq. (5b) is multiplied by $\sqrt{T}$ but the coefficients in Eq. (5) are the same as in Miki's original model.[2] Miki[11] has suggested that the three-parameter version of his model could be used to represent outdoor ground impedance. Horoshenkov *et al.*[15] have found good agreement between absorption coefficient data for soils and predictions of the three-parameter Miki model.[11]

In Ref. 10, it was shown that all surface impedance models in the square-root type family, including the variable porosity model, are physically admissible. It was also shown that the Delany and Bazley model for a semi-infinite ground can not satisfy both the reality and causality conditions and was thus not physically admissible. In its usual form, the Delany and Bazley model is used only on the basis that it satisfies the reality condition and is therefore not causal. In addition, for a rigidly backed layer, the real part of the surface impedance is negative at low frequencies, which violates the reality condition and is non physical. An example of this behavior is given in Fig. 1(a) for a rigidly backed layer of thickness $d = 1\,\mathrm{cm}$ and of air flow resistivity $\sigma = 100\,\mathrm{kPa\,s\,m^{-2}}$. The Miki model corrects the behavior of the Delany and Bazley model for a semi-infinite ground and is physically admissible. However, for a rigidly backed layer, it gives also a negative real part of the surface impedance at low frequencies, which shows that the Miki model is not physically admissible in this case. A modified Miki model was therefore proposed in Ref. 10 and was shown to be physically admissible for both types of surface impedances. Thus, it is observed in Fig. 1(a) that the real part of the surface impedance remains positive at low frequencies for the modified Miki model. The coefficients of the modified Miki model, along with those of the Delany and Bazley and Miki models, can be found in Table I.

At the same time, Kirby[16] investigated the properties of polynomial impedance models. He retrieved that the real part of the surface impedance for a rigidly backed layer using the Delany and Bazley and Miki models is negative at low frequencies. In addition, he showed also that these two models provide non-physical values for the density of the equivalent fluid given by

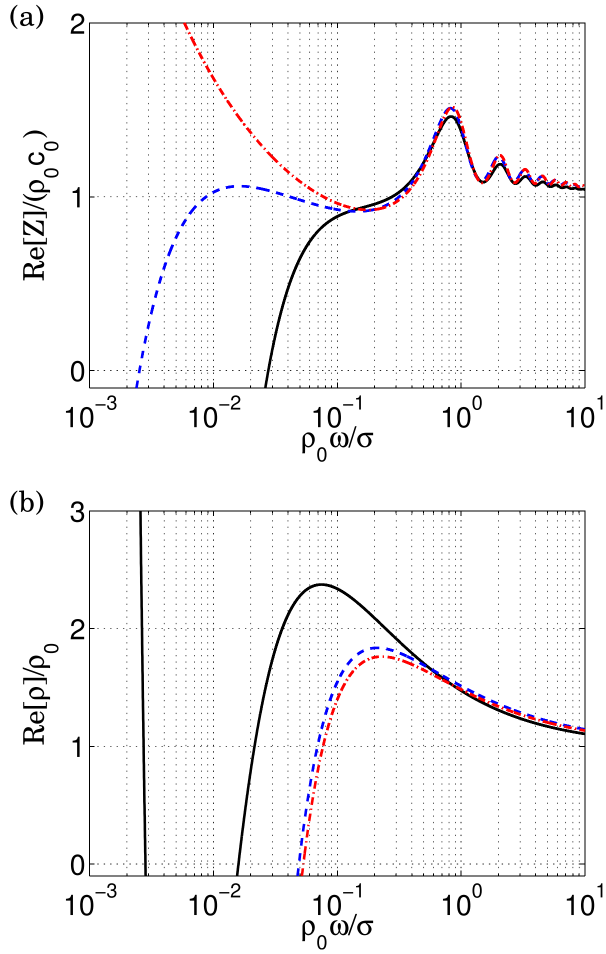

FIG. 1. (Color online) Real part (a) of the surface impedance and (b) of the complex density as a function of the normalized angular frequency $\rho_0\omega/\sigma$ for a rigidly backed layer of thickness $d = 1\,\mathrm{cm}$ and of air flow resistivity $\sigma = 100\,\mathrm{kPa\ s\ m^{-2}}$ and for (solid line) Delany and Bazley, (broken line) Miki, and (dashed-dotted line) modified Miki impedance models.

$$\rho = Z_c \frac{k_c}{\omega}, \tag{6}$$

as its real part is also negative at low frequencies. This is illustrated in Fig. 1(b) for the same set of coefficients used above. In addition to the three conditions described in (Conditions 1–3), a fourth condition for physical admissibility is therefore considered in this paper,

$$\text{Condition 4:} \quad \mathrm{Re}[\rho] \geq 0, \quad \text{for}\, \omega > 0.$$

This condition can be easily checked for the square-root type impedance models. Indeed, the density has a simple expression in this case,

$$\rho = \frac{\rho_0 T}{\Omega} \alpha\beta \left(1 + \frac{\omega_1}{-i\omega}\right). \tag{7}$$

Thus, the real part of the density is constant and positive for these models and the fourth condition is satisfied. As indicated above, the real part of the density can be negative at low frequencies for the Delany and Bazley and Miki models. This is also the case for the modified Miki model proposed in Ref. 10, as shown in Fig. 1(b). Indeed, using Eqs. (5) and the coefficients in Table I, the real part of the density for this model is given at low frequencies by

$$\mathrm{Re}[\rho] \underset{\omega \to 0}{\sim} \rho_0 (ap - cr) \left(\frac{\sigma}{\rho_0 \omega}\right)^{2b}. \tag{8}$$

As $ap - cr < 0$, this shows that the real part of the density is negative at low frequencies. While surface impedances for a semi-infinite ground and for a rigidly backed layer from the modified Miki model are physically admissible, this result indicates that the modified Miki model would give non-physical values for extended-reacting surfaces. This also tends to demonstrate that, while their use is simple as they depend on only one-parameter, polynomial models should not be used and more physically based impedance models should be preferred. Indeed, even if a polynomial model can be patched to give physically admissible results in particular cases, it must not be expected to give accurate values in the general case.

B. Tests for the slit-pore impedance model

In this section, the conditions for physical admissibility are checked for the slit pore model. The characteristic impedance Z_c and the propagation constant for the slit pore model are given by the equations (see, e.g., Ref. 7)

$$Z_c = \sqrt{\frac{T}{\Omega^2} \frac{\rho'}{C}}, \tag{9a}$$

$$k_c = \omega \sqrt{T \rho' C}, \tag{9b}$$

where the complex density ρ' and compressibility C are

$$\rho' = \frac{\rho_0}{G(\lambda)}, \tag{10}$$

$$C = \frac{1}{\gamma P_0} \left[\gamma - (\gamma - 1) G\left(\lambda \sqrt{\mathrm{Pr}}\right)\right], \tag{11}$$

with P_0 the mean pressure and Pr the Prandtl number. These quantities depend on the function G defined by

$$G(\lambda) = 1 - \frac{\tanh\left(\lambda\sqrt{-i}\right)}{\lambda\sqrt{-i}}, \tag{12}$$

$$\lambda = \sqrt{\frac{3\rho_0 \omega T}{\Omega \sigma}}. \tag{13}$$

Using the relation $P_0 = \rho_0 c_0^2/\gamma$, Eq. (9) can be rewritten as

$$Z_c = Z_\infty \left[f_1\left(\sqrt{\frac{-i\omega}{\omega_1}}\right) f_2\left(\sqrt{\frac{-i\omega}{\omega_2}}\right)\right]^{-1/2}, \tag{14a}$$

$$k_c = \frac{\omega}{c_0} \sqrt{T} \left[f_2\left(\sqrt{\frac{-i\omega}{\omega_2}}\right) \Big/ f_1\left(\sqrt{\frac{-i\omega}{\omega_1}}\right)\right]^{1/2}, \tag{14b}$$

where the functions f_1 and f_2 are defined by

$$f_1(z) = 1 - \frac{\tanh z}{z}, \tag{15a}$$

$$f_2(z) = 1 + (\gamma - 1)\frac{\tanh z}{z}, \tag{15b}$$

and where the parameters of the model are given by $Z_\infty = \rho_0 c_0 \sqrt{T}/\Omega$, $\omega_1 = \Omega\sigma/(3\rho_0 T)$, and $\omega_2 = \Omega\sigma/(3\rho_0 T \mathrm{Pr}) = \omega_1 \epsilon^2$, with $\epsilon = 1/\sqrt{\mathrm{Pr}}$. The branch cut of the complex square root functions is chosen as the negative real axis.

For the slit pore model, Condition 4 is straightforwardly checked as $\rho = \rho' T/\Omega = T\rho_0/(\Omega f_1[\sqrt{-i\omega/\omega_1}])$. Indeed, from Eq. (B2) in Appendix B, $\mathrm{Re}[f_1] \geq$ for $\omega > 0$ which implies that $\mathrm{Re}[\rho] \geq 0$, for $\omega > 0$.

1. Semi-infinite ground

The slit-pore surface impedance model is first considered for a semi-infinite ground. It is straightforwardly seen that $Z_{S,\infty}$ is a real model (Condition 1) as $\overline{Z_{S,\infty}(\omega)} = Z_{S,\infty}(-\omega)$. It is also a passive model (Condition 2) as $\mathrm{Re}[Z_{S,\infty}(\omega)] \geq 0$ in the whole complex plane due to the square root function.

The causality condition (Condition 3) is now investigated. As $Z_{S,\infty}$ is singular for $\omega = 0$ and as it is not square-integrable on the real line (Conditions 3.a–3.c) are not directly checked for $Z_{S,\infty}$. Instead, one considers the function

$$A(\omega) = Z_{S,\infty} - Z_\infty \sqrt{\frac{3\omega_1}{-i\omega\gamma} \frac{\omega_1}{\omega_1 - i\omega}} - Z_\infty \left(1 + \frac{\sqrt{\omega_1} - (\gamma - 1)\sqrt{\omega_2}}{2\sqrt{\omega_1 - i\omega}}\right). \tag{16}$$

The second and third terms aim at removing the singularity due to $Z_{S,\infty}$ at $\omega = 0$ and at obtaining a square-integrable function, respectively. Indeed, for large $|\omega|$, $|A(\omega)|$ is behaving as $1/|\omega|$, which shows that $A(\omega)$ is square-integrable on the real line (Condition 3.a).

Then, it must shown that the function $A(\omega)$ is analytic in $\mathrm{Im}(\omega > 0)$ (Condition 3.b). Note that this is straightforwardly satisfied for all functions in $A(\omega)$ except $Z_{S,\infty}$. For $Z_{S,\infty}$, the function under the radical in Eq. (14a) must not cross the branch cut of the square root function in $\mathrm{Im}(\omega > 0)$. It is deduced from Eqs. (B4) in Appendix B that for $-\pi/4 \le \mathrm{Arg}(z) \le \pi/4$, $-\pi/2 \le \mathrm{Arg}[f_1 f_2] \le \pi/2$, which shows that $f_1 f_2$ do not cross the branch cut of the square root function in $\mathrm{Im}(\omega > 0)$. In addition, as discussed in Appendix B, the function f_1 has only one zero at $\omega = 0$ and f_2 has no zeroes in $\mathrm{Im}(\omega > 0)$. Therefore, the only singularity of $Z_{S,\infty}$ in $\mathrm{Im}(\omega > 0)$ is at $\omega = 0$ and $A(\omega)$ is analytic in $\mathrm{Im}(\omega > 0)$.

It remains to show that $A(\omega)$ is uniformly converging to 0 as $|\omega|$ tends to infinity for $0 \le \mathrm{Arg}(\omega) \le \pi$ (Condition 3.c). With this aim, the inequality

$$|A(\omega)| \le |Z_{S,\infty} - Z_\infty| + Z_\infty \sqrt{\frac{3\omega_1}{\gamma|\omega|}} \frac{\omega_1}{|\omega_1 - |\omega||} + Z_\infty \frac{\sqrt{\omega_1} - (\gamma - 1)\sqrt{\omega_2}}{2\sqrt{|\omega_1 - |\omega||}} \quad (17)$$

is first obtained. The second and third term in this equation are converging uniformly to 0 in $\mathrm{Im}(\omega) > 0$, as $|\omega| \to \infty$. This must then be shown for $|Z_{S,\infty} - Z_\infty|$. Using the inequality $|z-1|^2 \le |z^2 - 1|$ for $\mathrm{Re}(z) \ge 0$ (see, e.g., Ref. 10) one gets

$$|Z_{S,\infty} - Z_\infty|^2 \le Z_\infty^2 \left| \frac{(\gamma - 1)F(\epsilon K) - F(K) - (\gamma - 1)F(\epsilon K)F(K)}{[1 - F(K)][1 + (\gamma - 1)F(\epsilon K)]} \right| \le Z_\infty^2 \frac{(\gamma - 1)|F(\epsilon K)| + |F(K)| + (\gamma - 1)|F(\epsilon K)||F(K)|}{|1 - |F(K)|||1 - (\gamma - 1)|F(\epsilon K)||},$$

with $F(K) = \tanh(K)/K$ and $K = \sqrt{-i\omega/\omega_1}$. It is demonstrated from Eq. (A14) in Appendix A that $F(K)$ tends uniformly to 0 as $|K| \to \infty$ in $-\pi/4 \le \mathrm{Arg}(K) \le \pi/4$. Therefore, it is concluded that $Z_{S,\infty} - Z_\infty$ and thus $A(\omega)$ tend uniformly to 0 in $\mathrm{Arg}(\omega) \in [0, \pi]$ as $|\omega| \to \infty$. Finally, $A(\omega)$ satisfy (Condition 3) and is therefore a causal transform. As the other terms in Eq. (16) are also causal transforms,[17] it is deduced that $Z_{S,\infty}$ is a causal transform.

As a consequence, the slit pore model for a semi-infinite ground is physically admissible.

2. Rigidly backed layer

The physical admissibility of the surface impedance of a rigidly backed layer is now investigated. The reality condition (Condition 1) is straightforwardly checked, as $\overline{Z_{S,d}(\omega)} = Z_{S,d}(-\omega)$.

Concerning the passivity condition (Condition 2), it is first verified that $\mathrm{Re}[k_c] \ge 0$ and $\mathrm{Im}[k_c] \ge 0$ in $\omega > 0$. Using Eq. (B4a) in Appendix B, it is obtained that for $\omega > 0$, $-\pi/2 \le \mathrm{Arg}[f_1] \le 0$ and $0 \le \mathrm{Arg}[f_2] \le \pi/2$. This shows the inequality

$$0 \le \mathrm{Arg}\left[f_2\left(\sqrt{\frac{-i\omega}{\omega_2}}\right)\right] - \mathrm{Arg}\left[f_1\left(\sqrt{\frac{-i\omega}{\omega_1}}\right)\right] \le \pi, \quad (18)$$

which implies that $0 \le \mathrm{Arg}(k_c) = (\mathrm{Arg}[f_2] - \mathrm{Arg}[f_1])/2 \le \pi/2$ and, hence, $\mathrm{Re}[k_c] \ge 0$ and $\mathrm{Im}[k_c] \ge 0$ in $\omega > 0$. Therefore, using the inequality

$$\mathrm{Arg}[-iz] \le \mathrm{Arg}[\coth(-iz)] \le -\mathrm{Arg}[-iz], \quad (19)$$

which is valid for $\mathrm{Re}[z] > 0$ and $\mathrm{Im}[z] > 0$,[10] one obtains

$$\mathrm{Arg}[Z_c] + \mathrm{Arg}[-ik_c d] \le \mathrm{Arg}[Z_{S,d}] \le \mathrm{Arg}[Z_c] - \mathrm{Arg}[-ik_c d]. \quad (20)$$

This implies the inequality

$$-\frac{\pi}{2} - \mathrm{Arg}[f_1] \le \mathrm{Arg}[Z_{S,d}] \le \frac{\pi}{2} - \mathrm{Arg}[f_2], \quad (21)$$

which, from the preceding comments, yields $-\pi/2 \le \mathrm{Arg}[Z_{S,d}] \le \pi/2$. Therefore, the real part of $Z_{S,d}$ is positive, which demonstrates that the model of a rigidly backed layer is passive.

The causality condition (Condition 3) is now investigated. First, one shows that $\mathrm{Im}[k_c] > 0$ in $\mathrm{Im}(\omega) > 0$. For that, writing $\omega = |\omega| e^{i\theta}$, the argument of k_c is given by

$$\mathrm{Arg}[k_c] = \theta + \frac{1}{2}\left[\mathrm{Arg}[f_2](K) - \mathrm{Arg}[f_1](\epsilon K)\right], \quad (22)$$

with $K = \sqrt{-i\omega/\omega_1}$. For $0 \le \theta \le \pi/2$, one has $-\pi/4 \le \mathrm{Arg}[K] \le 0$ which from Eq. (B4a) in Appendix B yields $0 \le \mathrm{Arg}[k_c] \le \pi$. This shows that $\mathrm{Im}(k_c) > 0$ in $\mathrm{Arg}(\omega) \in [0; \pi/2]$. Similarly, for $\pi/2 \le \theta \le \pi$, from Eq. (B4b) in Appendix B, one has $0 \le \mathrm{Arg}[k_c] \le \pi$, which finally shows that $\mathrm{Im}(k_c) > 0$ in $\mathrm{Arg}(\omega) \in [\pi/2; \pi]$ and, hence, in $\mathrm{Arg}(\omega) \in [0; \pi]$.

This property allows us to consider the function $Z_{S,d}^{(n)} = Z_{S,\infty} e^{2ink_c d}$ to demonstrate that the impedance model of a rigidly backed layer is causal.[10] However, $Z_{S,d}^{(n)}$ is not square-integrable on the real-axis as it is singular at $\omega = 0$. As done in Sec. II B 1, one considers instead the function $B(\omega) = B_1(\omega) - B_2(\omega)$, with

$$B_1(\omega) = Z_{S,d}^{(n)} e^{-i\omega t_n} - Z_{S,\infty} e^{-\sqrt{-i\omega\omega_3}t_n} e^{-\omega_4 t_n} e^{-\omega_5^{3/2}/\sqrt{-i\omega}t_n}, \quad (23a)$$

$$B_2(\omega) = Z_\infty \sqrt{\frac{3\omega_1}{-i\omega\gamma}} \frac{\omega_1}{\omega_1 - i\omega}[1 - e^{-\omega_4 t_n}], \tag{23b}$$

with $t_n = 2nd\sqrt{T}/c_0$, $\sqrt{\omega_3} = (\sqrt{\omega_1} + (\gamma - 1)\sqrt{\omega_2})/2$, $\omega_4 = \sqrt{\omega_1\omega_3} - \omega_3/2$, and $\omega_5^{3/2} = \omega_1\sqrt{\omega_3} - \sqrt{\omega_1}\omega_3 + \omega_3^{3/2}/2$. As for a semi-infinite ground, B_2 aims at removing the singularity of $Z_{S,d}^{(n)}$ at $\omega = 0$. The function B is square-integrable over the real axis, as B_1 and B_2 decay as $e^{-\sqrt{|\omega|\omega_3/2}t_n}$ and $|\omega|^{-3/2}$ for large $|\omega|$, respectively. (Condition 3.b) is thus fulfilled. In addition, B is analytic in $\mathrm{Im}[\omega] > 0$ (Condition 3.a). Indeed, in $\mathrm{Im}[\omega] > 0$, the function under the radical in Eq. (14b) do not cross the branch cut of the square root function from Eqs. (B4) in Appendix B. In addition, the branch cuts of the square root functions in B are located in the ω-plane along the line $\mathrm{Re}(\omega) = 0$ and $\mathrm{Im}(\omega) < 0$ and the pole in $\mathrm{Im}[\omega] < 0$. Finally, one must then show that B is uniformly converging to 0 as $|\omega| \to \infty$ for $\mathrm{Arg}(\omega) \in [0;\pi]$ (Condition 3.c). Note that it is the case for B_2 as discussed in Sec. II B 1. Therefore, it remains to show this property for B_1. First, B_1 is rewritten as

$$B_1(\omega) = Z_{S,\infty} e^{-\sqrt{-i\omega\omega_3}t_n} e^{-\omega_4 t_n} e^{-\omega_5^{3/2}/\sqrt{-i\omega}t_n}[e^{i\omega(x-y)t_n} - 1], \tag{24}$$

with

$$x = \left[f_2\left(\sqrt{\frac{-i\omega}{\omega_2}}\right) \Big/ f_1\left(\sqrt{\frac{-i\omega}{\omega_1}}\right)\right]^{1/2}, \tag{25}$$

$$y = 1 + \sqrt{\frac{\omega_3}{-i\omega} + \frac{\omega_4}{-i\omega} + \left(\frac{\omega_5}{-i\omega}\right)^{3/2}}. \tag{26}$$

A first upper bound is obtained with

$$|B_1(\omega)| \le Z_{S,\infty} e^{-\sqrt{|\omega|\omega_3/2}t_n} e^{-\omega_4 t_n} \times e^{-\omega_5^{3/2}/\sqrt{2|\omega|}t_n} |e^{i\omega(x-y)t_n} - 1|. \tag{27}$$

Simplifying and using the relation $|e^z - 1| \le |z|e^{|z|}$,[17] one gets

$$|B_1(\omega)| \le Z_{S,\infty} e^{-\sqrt{|\omega|\omega_3/2}t_n} |\omega||x - y| t_n e^{|\omega||x-y|t_n}. \tag{28}$$

As $e^{-\sqrt{|\omega|\omega_3/2}t_n}$ is uniformly converging to 0, it remains to show that $|\omega||x - y|$ is uniformly bounded as $|\omega| \to \infty$ for $\mathrm{Arg}(\omega) \in [0;\pi]$. First, note that $\mathrm{Re}[x/y] \ge 0$ for sufficiently large $|\omega|$ in $\mathrm{Im}[\omega] \ge 0$. Indeed, from comments given in Appendix B, $\mathrm{Re}(x) \ge 0$ and $\mathrm{Im}(x) \ge 0$ for $\mathrm{Arg}(\omega) \in [0;\pi/2]$ and $\mathrm{Re}(x) \ge 0$ and $\mathrm{Im}(x) \le 0$ for $\mathrm{Arg}(\omega) \in [\pi/2;\pi]$. In addition, the terms in y have the same properties except the term $(\omega_5/(-i\omega))^{3/2}$ which has a negative real part for $\mathrm{Arg}(\omega)$ close to 0 and to π. This shows that $\mathrm{Re}(x)\mathrm{Re}(y) + \mathrm{Im}(x)\mathrm{Im}(y) \ge 0$ for sufficiently large $|\omega|$, which leads to $\mathrm{Re}[x/y] \ge 0$. Using the relation $|z - 1|^2 \le |z^2 - 1|$ for $\mathrm{Re}(z) \ge 0$, as in Sec. I, yields

$$|x - y| \le |x^2 - y^2|^{1/2}. \tag{29}$$

In addition, one has

$$|x^2 - y^2| \le \frac{1}{|1 - |\tanh(\epsilon K)/(\epsilon K)||} \left[\frac{\gamma - 1}{|\epsilon K|}|\tanh(\epsilon K) - 1| + \frac{1}{|K|}|\tanh(K) - 1| + \frac{1 + (\gamma - 1)\epsilon}{|K|^2}|\tanh(K) - 1| + \frac{1 + (\gamma - 1)\epsilon}{|K|^3}|\tanh(K) - 1| + \frac{1}{|K|^4}\left(g_4(\epsilon)|\tanh(K)| + h_4(\epsilon)\right) + \frac{1}{|K|^5}\left(g_5(\epsilon)|\tanh(K)| + h_5(\epsilon)\right) + \frac{1}{|K|^6}\left(g_6(\epsilon)|\tanh(K)| + h_6(\epsilon)\right) + \frac{g_7(\epsilon)}{|K|^7}|\tanh(K)|\right], \tag{30}$$

where g_4, g_5, g_6, g_7, h_4, h_5, and h_6 are functions of ϵ. The function $\tanh(z)/z$ is uniformly converging to 0, and the function $\tanh(z)$ is uniformly and exponentially converging to 1, as indicated in Eqs. (A14) and (A17). This shows that $|\omega||x - y| \le |\omega||x^2 - y^2|^{1/2} \le G(K)$, where $G(K)$ is a function uniformly converging to $(g_4(\epsilon) + h_4(\epsilon))\omega_1$ as $|K| \to \infty$. Therefore, $|\omega||x - y|$ is uniformly bounded in $\mathrm{Im}[\omega] \ge 0$ as $|\omega| \to \infty$, and, hence, B_1 is uniformly converging to 0 in $\mathrm{Im}[\omega] \ge 0$ as $|\omega| \to \infty$. It is concluded that B is a causal transform. B_2 is a causal transform as discussed in Sec. II B 1. The term $Z_{S,\infty} e^{-\sqrt{-i\omega\omega_3}t_n} e^{-\omega_4 t_n} e^{-\omega_5^{3/2}/\sqrt{-i\omega}t_n}$ in B_1 is also causal as it is the product of three causal transforms, the first one being $Z_{S,\infty}$, as shown in Sec. II B 1, the second one $e^{-\sqrt{-i\omega\omega_3}t_n}$ (see Ref. 17), and the third one $e^{-\omega_5^{3/2}/\sqrt{-i\omega}t_n}$. Indeed, the last transform is causal as it can be rewritten as

$$e^{-\sqrt{\omega_0/(-i\omega)}} = \sum_{k=0}^{\infty} \frac{(-1)^k}{k!}\left(\frac{-i\omega}{\omega_0}\right)^{-k/2}, \tag{31}$$

with $\omega_0 = \omega_5^3 t_n^2$. As, the inverse Fourier transform of $(-i\omega)^{-p}$ for $p > 0$ is causal,[17] the inverse Fourier transform of $e^{-\omega_5^{3/2}/\sqrt{-i\omega}t_n}$ is also causal. Therefore, $Z_{S,d}^{(n)} e^{-i\omega t_n}$ is a causal transform. As its inverse Fourier transform is $z_{S,d}^{(n)}(t + t_n)$, it is deduced that $z_{S,d}^{(n)}(t)$ is null for $t < t_n$ and hence is causal. Finally, $Z_{S,d}$ is also a causal transform by linearity.[10]

As a consequence, the slit pore model for a rigidly backed layer satisfies (Conditions 1–3) and is thus physically admissible.

III. COMPARISONS WITH SHORT RANGE DATA

NT ACOU 104 Ground surfaces: Determination of the Acoustic Impedance[4] describes the fitting of predictions based on the Delany and Bazley impedance model to third-octave data for the difference in levels recorded between vertically separated microphones at a short distance from a point source (source height 0.5 m, receiver heights at 0.5 and 0.2 m, separation 1.75 m). The fits are used to categorise a given ground surface in terms of twelve impedance classes based on values of effective flow resistivity. Figures 2(a) and 2(b) show data obtained in connection with NT ACOU 104 (Ref. 18) and best-fit predictions of the Delany and Bazley, modified Miki and variable porosity[7] impedance models for two grass covered ground surfaces.

In a similar way to the procedure used in NT ACOU 104,[4] the fitting errors (E) of the predictions have been determined from

$$\mathrm{E} = \sum_{f} [\mathrm{LD_M}(f) - \mathrm{LD_C}(f)], \tag{32a}$$

$$\mathrm{LD_C} = \mathrm{EA}(1) - \mathrm{EA}(2), \tag{32b}$$

$$\mathrm{EA}(1) = 20\,\mathrm{lg}\left|1 + \frac{QR_1}{R_2} e^{ik(R_2 - R_1)}\right|, \tag{32c}$$

$$\mathrm{EA}(2) = 20\,\mathrm{lg}\left|1 + \frac{QR_3}{R_4} e^{ik(R_4 - R_3)}\right|. \tag{32d}$$

In Eqs. (32a) and (32b), $\mathrm{LD_M}$ and $\mathrm{LD_C}$ are, respectively, the measured and predicted level difference magnitudes between microphones at distances R_1 and R_3 from the source and to which the corresponding ground-reflected ray path lengths are R_2 and R_4. In Eqs. (32c) and (32d), EA(1) and EA(2) are the predicted excess attenuation magnitudes and Q is the spherical wave reflection coefficient which depends on the surface impedance and the source-receiver geometry according to Eqs. (33a)–(33d),

$$Q = R_p + (1 - R_p)F(w), \tag{33a}$$

$$R_p = \frac{\cos\theta - \beta}{\cos\theta + \beta}, \tag{33b}$$

$$F(w) = 1 + i\sqrt{\pi} w \exp(-w^2)\mathrm{erfc}(-iw), \tag{33c}$$

$$w = \sqrt{ikR_2}(\cos\theta + \beta) \text{ or } w = \sqrt{ikR_4}(\cos\theta + \beta), \tag{33d}$$

where θ is the (specular) angle of incidence, β is the surface admittance, and $\mathrm{erfc}(\cdots)$ is the complementary error function.

Strictly, the level difference magnitude is not exactly the same as the difference in two excess attenuation magnitudes since the direct path lengths to the two receivers (R_1 and R_3) are not the same. However, since only the magnitude of the level difference is used in the comparisons with data, the approximation in Eq. (32b) is unimportant. Another factor with respect to the comparisons between data and predictions in Figs. 2 and 3 is that the data are in third octave bands whereas the predictions are at more closely spaced frequencies. The fitting errors listed in Table II represent the arithmetic sum of the spectral differences between predicted

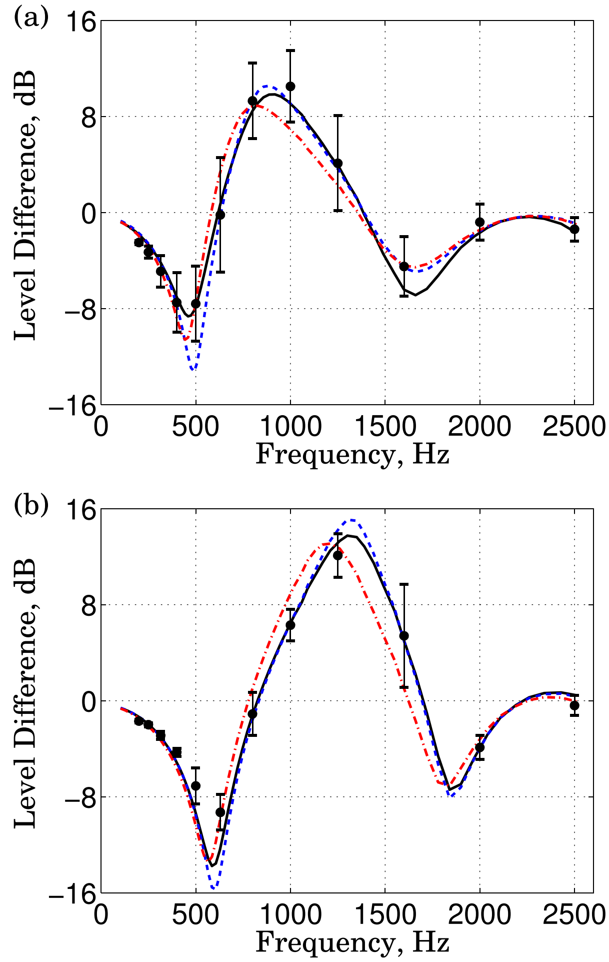

FIG. 2. (Color online) NORDTEST third octave band level difference data (•) [error bars indicate 90% confidence limits (±1.65 standard deviation (SD))] and best fit predictions (a) for long grass (site #20) (Ref. 18) using the variable porosity model (Ref. 7) (solid line, effective flow resistivity 20 kPa s m^{-2} and porosity rate 50/m); the Delany and Bazley layer model (broken line, effective flow resistivity 110 kPa s m^{-2} and effective layer depth 0.019 m); and the modified Miki layer model (dashed-dotted line, effective flow resistivity 100 kPa s m^{-2} and effective layer depth 0.025 m) and (b) for lawn (site #30) (Ref. 18) using the variable porosity model (Ref. 7) (solid line, effective flow resistivity 366.5 kPa s m^{-2} and porosity rate −79.5/m); the Delany and Bazley model (broken line, effective flow resistivity 746 kPa s m^{-2}); and the modified Miki model (dashed-dotted line, effective flow resistivity 565 kPa s m^{-2}).

and measured spectra at the third octave band centre frequencies between 100 Hz and 2.5 kHz. Although affecting the absolute error values, this simplification does not affect the indication they give of the relative goodness of fit. For example, the fitting errors to NORDTEST long grass site #20 short range data for the variable porosity and Delany and Bazley layer models obtained after correcting the narrow band predictions to third octave predictions are 7.0 and 11.5 dB, respectively.[7] While use of either the Delany and Bazley or the Miki impedance models enables reasonably good fits to these grassland data, as is the case for many other examples[7] use of the two-parameter variable porosity impedance model yields better fits.

Figures 3(a) and 3(b) show short range level difference data for a beech forest floor and gravel in a pit, respectively, and best-fit predictions using the Delany and Bazley, modified Miki, three parameter Miki, and slit pore[7] hard-backed

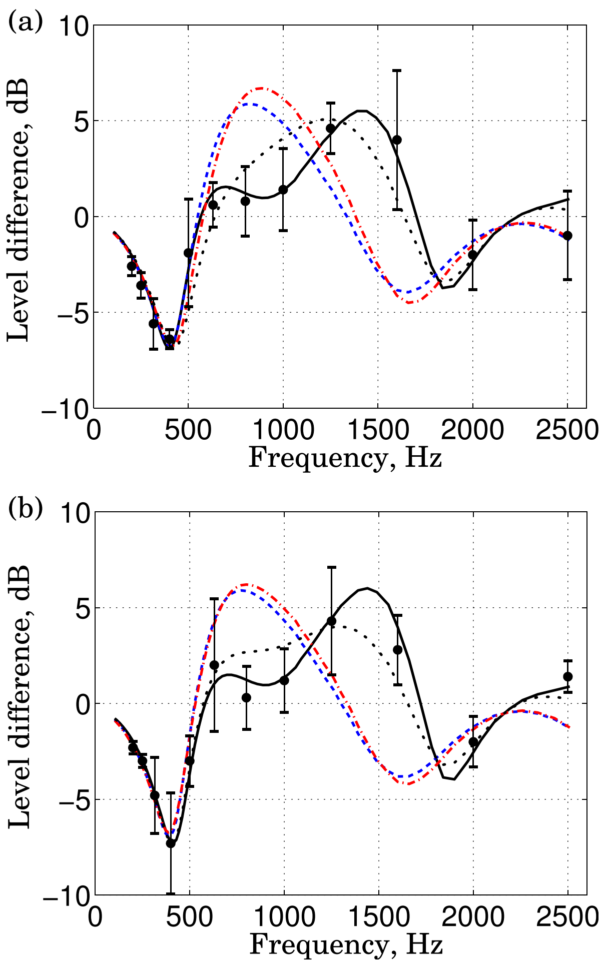

FIG. 3. (Color online) NORDTEST third octave band level difference data (•) (a) for a beech forest floor (site #36) and (b) for gravel in a pit (site #38) (Ref. 18) [error bars indicate 90% confidence limits (±1.65 SD)]. Also shown are best fit predictions using the slit pore layer model [solid lines: effective flow resistivity (a) 31.9 kPa s m^{-2}, (b) 33.6 kPa s m^{-2}; porosity (a) 0.35, (b) 0.33; effective layer depth (a) 0.07 m, (b) 0.068 m]; the Delany and Bazley layer model [broken lines: effective flow resistivity (a) 61.4 kPa s m^{-2}, (b) 55 kPa s m^{-2}; effective layer depth 0.04 m for (a) and (b)]; modified Miki layer model [dashed-dotted lines: effective flow resistivity (a) 90 kPa s m^{-2}, (b) 50 kPa s m^{-2}; effective layer depth 0.04 m for (a) and (b)]; and the three-parameter Miki layer model [dotted lines, effective flow resistivity (a) 18 kPa s m^{-2}, (b) 13.8 kPa s m^{-2}; porosity (a) 0.46, (b) 0.462; effective layer depth (a) 0.056 m, (b) 0.057 m].

layer impedance models. The corresponding fitting errors are listed also in Table II. Comparable third octave band corrected errors for the gravel in a pit site #38 data are 3.7 and 22.3 dB using the slit pore layer and Delany and Bazley layer models, respectively.[7] The structure of the measured spectra in Fig. 3 is found in the data for four of the sites considered in Ref. 7 which are intended as representative of deciduous forest floor and gravel sites. According to Ref. 19, the Delany and Bazley model (semi-infinite or hard back layer) fails to enable qualifying fits to short range data for 18 of 44 sites. The majority of these sites are forest floors and gravel with relatively low flow resistivities. For calculations involving the three-parameter form of the Miki model and the slit pore impedance model, the relationship $T = 1/\sqrt{\Omega}$ is assumed.[7] This means that both the slit pore and three-parameter Miki models require only two parameters (effective flow resistivity and porosity) for semi-infinite layers and the layer depth as a third parameter if the hard-backed layer versions are used [through Eq. (2)]. Nevertheless the description "three-parameter" is retained to describe the relevant version of the Miki model. In fitting predictions using the hard-backed layer versions of the slit pore model and the three-parameter form of the Miki model, the flow resistivity, porosity and layer depth were varied independently.

It was shown in Ref. 7 that the variable porosity model, despite providing superior fits for grassland, does not fit these short range forest floor and gravel data as well as the one parameter models so the fits using the variable porosity model are not shown in Figs. 3(a) and 3(b). Use of the three-parameter form of the Miki model to represent the ground impedance enables significantly better fits to short range data for lower flow resistivity surfaces (such as forest floors and gravel) than obtained with the Delany and Bazley and modified Miki models. However, using the semi-infinite and hard-backed slit pore layer models it is possible to obtain even better fits.

IV. COMPARISONS OF PREDICTIONS OVER GRASSLAND AT LONGER RANGE

A. Frequency-domain predictions

Although the fits to short range level difference magnitude data for grassland sites #20 and #30 shown in Figs. 2(a) and 2(b) are comparably good and would qualify for site classification according to the NORDTEST criteria, they are associated with the rather different impedance spectra shown in Figs. 4(a) and 4(b). Incidentally, it should be noted that the Delany and Bazley layer model predicts a negative real part of surface impedance below 150 Hz when using the best fit parameters for long grass.

Figure 5 illustrates the resulting differences in excess attenuation (EA) spectra predicted for a source height of 1 m a receiver height of 1.5 m and a range of 100 m that result from using three impedance models and the parameter values giving the best fits to short range data shown in Figs. 2(a) and 2(b). The predictions use Eqs. (34a)–(34f) which assume Gaussian turbulence[20]

$$L_p = 10\log_{10}[\langle p^2\rangle], \tag{34a}$$

$$\langle p^2\rangle = \frac{1}{R_1^2} + \frac{|Q|^2}{R_2^2} + \frac{2|Q|}{R_1R_2}\cos[k(R_2-R_1)+\theta]T, \tag{34b}$$

$$T = e^{-\sigma^2(1-\rho)}, \tag{34c}$$

$$\sigma^2 = A\sqrt{\pi}\langle\mu^2\rangle k^2 R L_0, \tag{34d}$$

$$A = 0.5 \quad R > kL_0^2, \tag{34e}$$

$$\text{or}\, A = 1.0 \quad R < kL_0^2, \tag{34f}$$

where θ is the phase of the spherical wave reflection coefficient, ($Q = |Q|e^{i\theta}$), T is the coherence factor determined by the turbulence effect, σ^2 is the variance of the phase fluctuation along a path, ρ is the phase covariance between adjacent

TABLE II. Errors in fitting short range propagation NORDTEST level difference spectra for five types of porous ground (Ref. 18) calculated using Eqs. (32) and (33) and various impedance models.

Ground type	Impedance model	Error (dB)
Long grass (site #20) (Ref. 18)	Variable porosity (Ref. 7)	9.7
	Delany and Bazley layer	12.1
	Modified Miki layer	13.6
Lawn (site #30) (Ref. 18)	Variable porosity (Ref. 7)	10.2
	Delany and Bazley	13.9
	Modified Miki	15.2
Pine forest floor (site #5) (Ref. 18)	Slit pore	4.9
	Delany and Bazley	19.8
	Modified Miki	21.5
	Three-parameter Miki	8.6
Beech forest floor (site #36) (Ref. 18)	Slit pore layer	8.7
	Delany and Bazley layer	26.7
	Modified Miki layer	27.6
	Three-parameter Miki layer	16.8
Gravel in a pit (site #38) (Ref. 18)	Slit pore layer	6.8
	Delany and Bazley layer	26.6
	Modified Miki layer	26.6
	Three-parameter Miki layer	14.4

paths (e.g., direct and reflected), $\langle \mu^2 \rangle$ is the variance of the index of refraction, R is the horizontal range, and L_0 is the outer scale of turbulence. The predictions assume moderate turbulence (refractive index variance $\langle \mu^2 \rangle = 10^{-6}$ and outer length scale $L_0 = 1$ m).

Use of the (physically inadmissible) Delany and Bazley and modified Miki impedance models with parameter values that yield best fits at short range for the NORDTEST long grass and lawn sites leads to substantial differences in predictions at 100 m range, particularly at and below 500 Hz, to those obtained using physically admissible models that enable better fits at short range. Predictions of signal waveforms at 100 m range allowing for refraction rather than turbulence and based on parameter values corresponding to the short range data fits in Figs. 2(a) and 2(b) are considered in Sec. IV B.

Spatial and seasonal variations of ground impedance for three types of ground: an artificial grass football (soccer) pitch, a grass lawn and a "natural" grass-covered ground have been reported by Guillaume *et al.*[12] At each site measurements were made at a series of locations of spectra of the level difference between vertically separated microphones at heights of 0.6 and 0 m at a distance of 4 m from an omnidirectional source at height of 0.6 m. Measurement campaigns were carried out in summer and winter when the grounds were dry and moist, respectively. The resulting level difference data were fitted using hard-backed layer versions of two semi-empirical impedance models (Delany and Bazley and Miki), the fitted parameters are effective flow resistivity and effective layer thickness. The Delany and Bazley model predictions for both the artificial grass and the grass lawn were found to include negative real parts of the fitted impedance at frequencies below 100 Hz. Although the Miki model was found to predict positive values for the real part of fitted impedance of these surfaces, the original Miki model coefficients and exponents were used. As discussed elsewhere,[10,15]

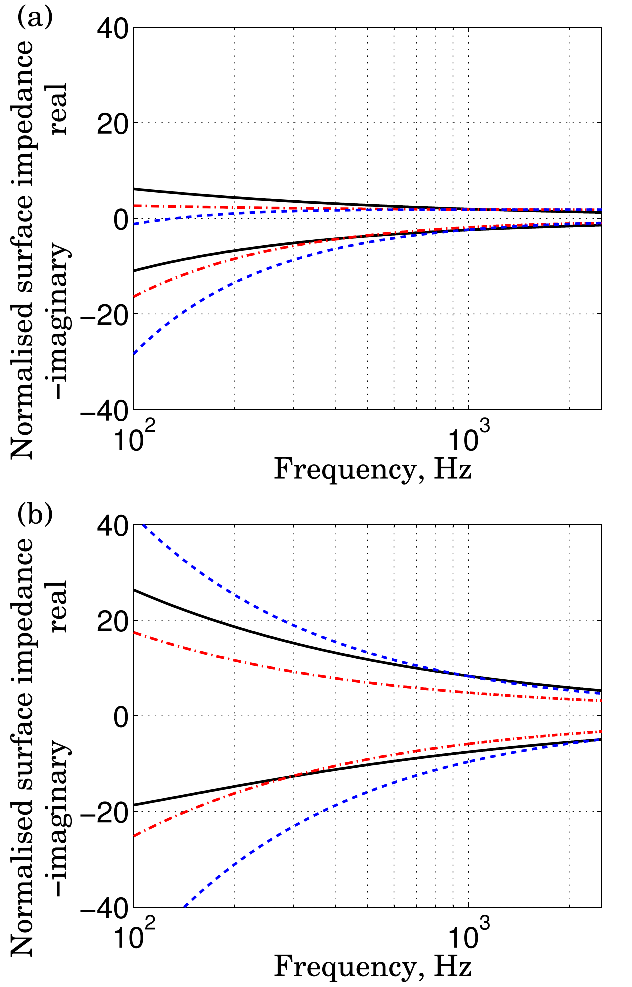

FIG. 4. (Color online) Impedance spectra corresponding to the best fits to short range level difference for (a) long grass, NORDTEST site #20 [Fig. 2(a)] and (b) lawn, NORDTEST site #30 [Fig. 2(b)] in Fig. 2. The line types correspond to the impedance models in the same way as those in Figs. 2(a) and 2(b).

despite its intention, the original Miki model leads to physically-inadmissible predictions at low frequencies. Nevertheless the parameter values resulting from fits using the Miki model with the original coefficients and exponents are reported in the analysis here.

The variable porosity model has been shown to be physically admissible[10] and to give good fits to many short range measurements over grassland [Figs. 2(a) and 2(b) and Ref. 7]. For easier comparison between the equivalent variable porosity parameter values and the best fit Miki layer model parameters, the second of the two parameters in the variable porosity model is interpreted as effective layer thickness d_e rather than porosity rate α_e ($d_e = 4/\alpha_e$).[7]

Table III lists mean, maximum, and minimum (original) Miki hard-backed layer model parameter values fitted to the measured level difference spectra.[12] The level difference spectra predicted for the short range measurement geometry using the Miki layer model have been fitted using the variable porosity model. The resulting parameter values are listed in Table III also.

Figure 6(a) shows an example of the short range level difference magnitude spectra predicted by the Miki model

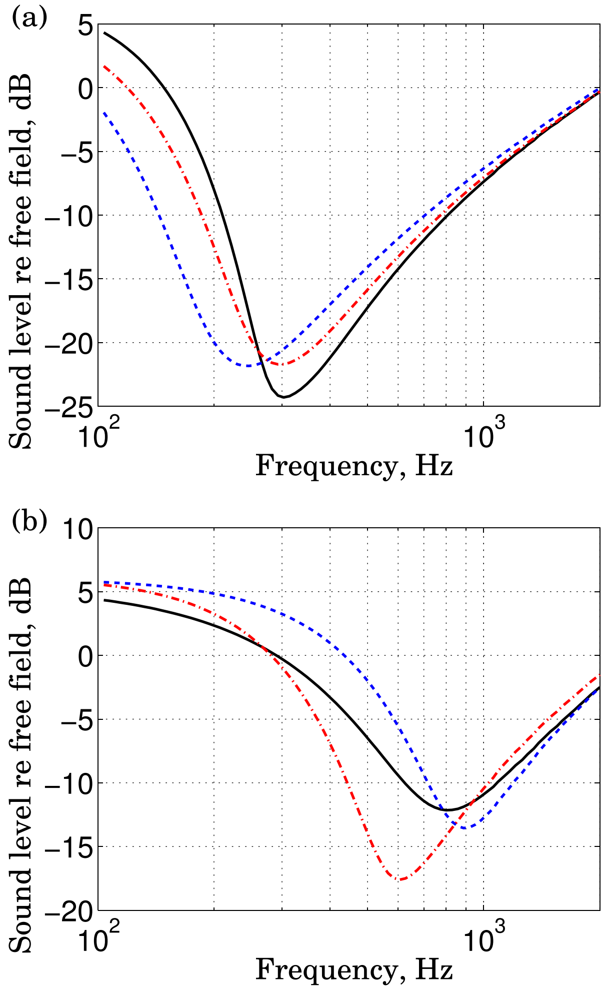

FIG. 5. (Color online) Comparisons of excess attenuation spectra in a turbulent atmosphere ($\langle \mu^2 \rangle = 10^{-6}$, $L_0 = 1$ m) for source height 1 m, receiver height 1.5 m, and range 100 m using impedance models and parameter values (see Table II) giving best fits to short range data obtained over (a) long grass, NORDTEST site #20 [Fig. 2(a)] and (b) lawn, NORDTEST site #30 [Fig. 2(b)]. The line types correspond to those in Figs. 2(a) and 2(b).

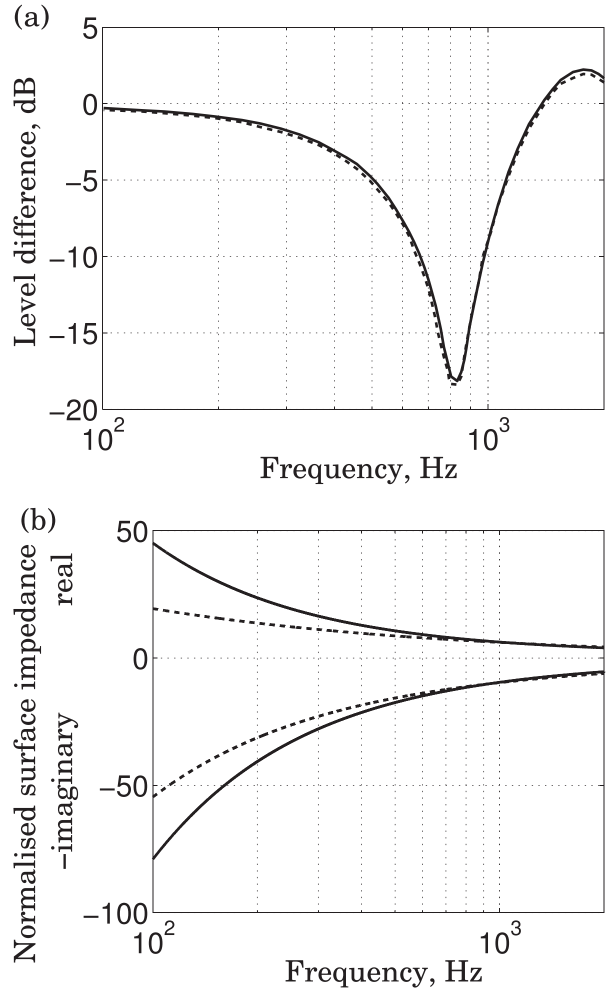

FIG. 6. (a) Level difference spectra predicted for the short range geometry used by Guillaume *et al.* (Ref. 12) using the Miki (solid line) and variable porosity (broken line) models with the parameter values for the mean winter grass lawn listed in Table III and (b) the corresponding predicted impedance spectra [line types as for (a)].

TABLE III. Mean, maximum, and minimum Miki parameter values that give best fits to the level difference spectra measurements over a grass lawn and "natural" grassland (Ref. 12) and the equivalent variable porosity impedance model parameters that yield nearly identical level difference magnitude predictions for the short range measurement geometry.

	Miki model parameters value				Variable porosity model parameters value			
	Summer		Winter		Summer		Winter	
Season/ Ground	Effective flow resistivity (kPa s m^{-2})	Effective thickness (m)	Effective flow resistivity (kPa s m^{-2})	Effective thickness (m)	Effective flow resistivity (kPa s m^{-2})	Effective thickness (m)	Effective flow resistivity (kPa s m^{-2})	Effective thickness (m)
Grass lawn								
Mean	354	0.0157	732	0.0058	80	0.035	200	0.011
Maximum	510	0.0116	990[a]	0.0042	105	0.023	285	0.008
Minimum	246	0.0138	409	0.0082	60	0.035	115	0.018
Natural ground								
Mean	173	0.0183	243	0.0158	40	0.042	55	0.037
Maximum	355	0.0148	460	0.0127	60	0.035	110	0.028
Minimum	73	0.025	75	0.026	19.3	0.055	20	0.062

[a]The value of 990 kPa s m^{-2} is the maximum permitted for effective flow resistivity in the fitting process (Ref. 12). It is stated as the "best fit" value for six of the winter measurements over the grass lawn.

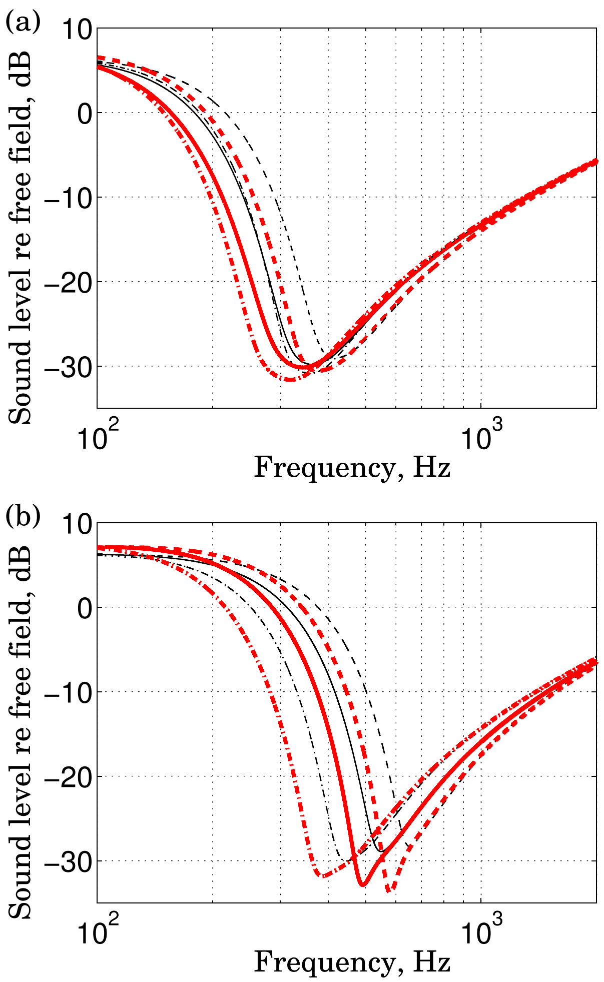

FIG. 7. (Color online) Predictions of the excess attenuation between a point source and a receiver, both at heights of 2 m and separated by a distance of 500 m, above a grass lawn in (a) summer and (b) winter, using the Miki impedance model (thin lines) and the variable porosity impedance model (thick lines) and the corresponding mean (solid lines), maximum (broken lines) and minimum (dashed-dotted lines) parameter values listed in Table III.

with the mean winter grass lawn parameters listed in Table III and the best fit predictions obtained using the variable porosity model using the relevant parameter values in Table III. Figure 6(b) shows the predictions of the corresponding impedance spectra. Again it should be noted that, while the predicted level difference magnitude spectra are nearly identical, the predicted impedance spectra are significantly different.

Since fewer measurements were made over the artificial grass and, in any case it is less representative of typical grassland of interest to outdoor sound predictions, only predictions using the best fit grass lawn and "natural" ground parameters are considered further.

The overall seasonal change in the short range level difference spectra between summer and winter conditions was found to be greater than the spatial variability at both sites and this is reflected in the parameter values listed in Table III. The parameters corresponding to the grass lawn show more seasonal variation than those for the "natural" ground. The ranges of mean effective flow resistivity for the grass lawn and grass-covered natural ground, according to the variable porosity model (60 to 200 kPa s m^{-2} and 19.3 to 110 kPa s m^{-2}, respectively), are at the lower end of the range for 26 grass-covered grounds (21.7 to 1296 kPa s m^{-2}) reported elsewhere.[7]

Figures 7 and 8 show that, at a long range, use of the variable porosity model with parameters that give rise to short range level difference spectra more or less identical to those predicted using the Miki model best fits result in predictions of larger ground effect maxima at lower frequencies than predicted using the Miki model. The predictions of excess attenuation spectra in Figs. 7 and 8 allow only for very weak turbulence (Gaussian: mean variance 10^{-10}, outer scale length 1 m)[20] since the comparable plots of predictions based on the original Miki model in Ref. 12 do not include turbulence effects. The differences between 500 m range excess attenuation predictions caused by use of the different impedance models are greater than those due to the observed spatial variations at either grassland site and comparable with those observed due to seasonal differences.

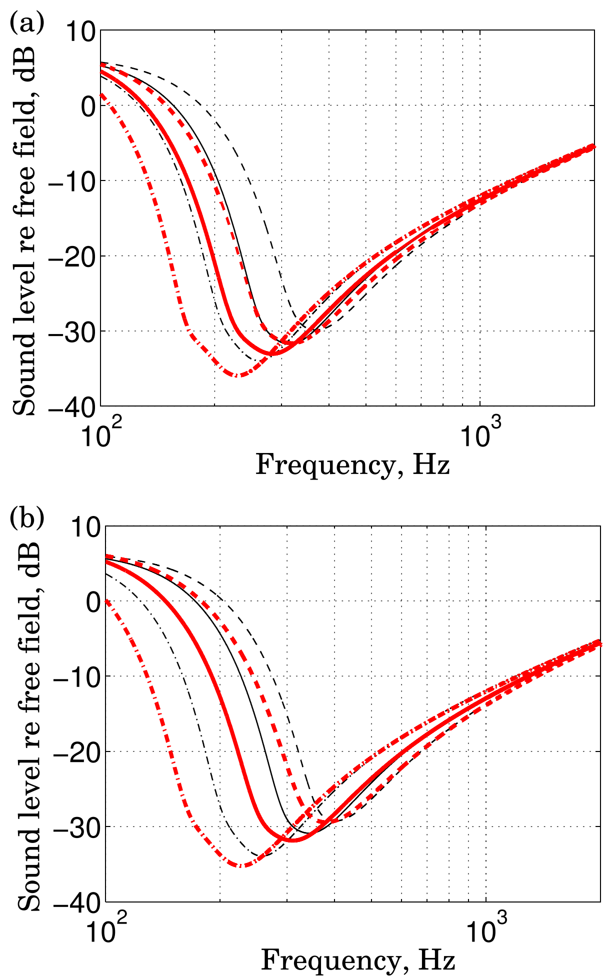

FIG. 8. (Color online) Predictions of the excess attenuation between a point source and a receiver, both at heights of 2 m and separated by a distance of 500 m, above a natural ground in (a) summer and (b) winter, using the Miki impedance model (thin lines) and the variable porosity impedance model (thick lines), with the respective mean (solid lines), maximum (broken lines), and minimum (dashed-dotted lines) parameter values listed in Table III.

B. Time-domain predictions

In this section, time-domain predictions of the sound propagation in an inhomogeneous atmosphere over impedance planes are performed, using the impedance models obtained from the short range data in Sec. III. For that, a time-domain solver of the linearized Euler equations presented in Refs. 21 and 22 is employed. A three-dimensional geometry (x, y, z) is considered with a domain size of $[-5\,\mathrm{m};\ 105\,\mathrm{m}] \times [-13.8\,\mathrm{m};\ 13.8\,\mathrm{m}] \times [0\,\mathrm{m};\ 20\,\mathrm{m}]$. The spatial derivatives are evaluated using the Fourier pseudospectral method in the horizontal directions, i.e., in the x- and y-direction, with constant spatial steps $\Delta x = \Delta y = 0.14\,\mathrm{m}$ and optimized finite-difference schemes[23] in the vertical direction, i.e., in the z-direction, with constant spatial step $\Delta z = 0.048\,\mathrm{m}$. The time step is set to $7 \times 10^{-5}\,\mathrm{s}$ and 4500 time iterations are performed. A time-domain impedance boundary condition is implemented at the ground.[21,24]

A logarithmic sound speed profile is considered:

$$c(z) = c_0 + a_c \log \frac{z + z_0}{z_0}, \tag{35}$$

with $z_0 = 0.1\,\mathrm{m}$ and a_c is set to $-2\,\mathrm{m\ s^{-1}}$ for an upward-refracting atmosphere and to $2\,\mathrm{m\ s^{-1}}$ for a downward-refracting atmosphere. The acoustic pressure p and velocity $\mathbf{v}$ are initialized by setting

$$p(\mathbf{r}, t = 0) = \rho_0 c_0^2 \exp\left(\frac{|\mathbf{r} - \mathbf{r_S}|^2}{B^2}\right), \tag{36a}$$

$$\mathbf{v}(\mathbf{r}, t = 0) = 0, \tag{36b}$$

where the source is centered at $\mathbf{r_S} = (0, 0, z_S)$, with $z_S = 1\,\mathrm{m}$ and with $B = 0.25\,\mathrm{m}$.

Figures 9 and 10 show the time series of the acoustic pressure at a receiver located at $x = 100\,\mathrm{m}$, $y = 0\,\mathrm{m}$, and $z = 2\,\mathrm{m}$ obtained using the impedance models and parameters values giving best fits over long grass, NORDTEST site #20, and lawn, NORDTEST site #30, respectively. Note that the Delany and Bazley model has been disregarded in these time-domain predictions as it is a non-causal model. For long grass, the time series obtained with the modified Miki model significantly differ from those obtained using the variable porosity models giving better fit. Thus, for a downward refracting atmosphere in Fig. 9(a), while the predicted first arrivals for t between 0.287 and 0.291 s present similar shapes, the peak

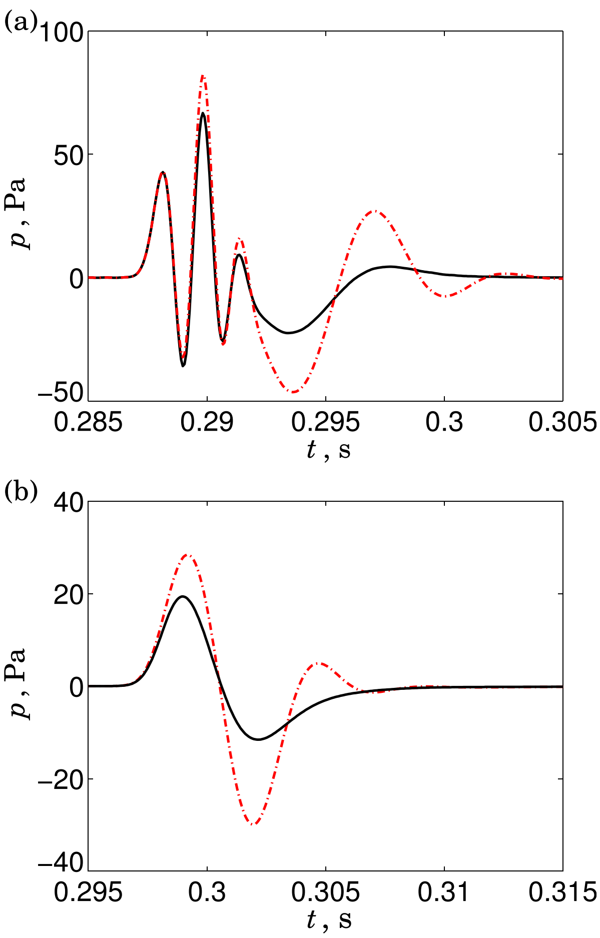

FIG. 9. (Color online) Time series at the acoustic pressure obtained at a receiver at $x = 100\,\mathrm{m}$, $y = 0\,\mathrm{m}$, and $z = 2\,\mathrm{m}$ (a) for a downward-refracting and (b) an upward-refracting atmosphere using impedance models and parameters values (see Table II) giving best fits to short range data obtained over long grass, NORDTEST #20: (solid line) variable porosity and (dashed-dotted line) modified Miki impedance models.

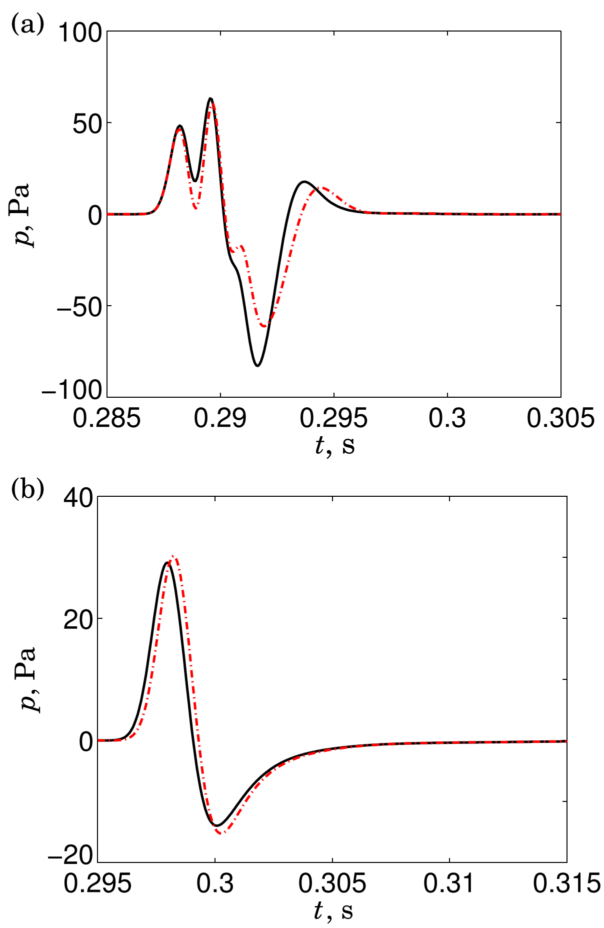

FIG. 10. (Color online) Time series at the acoustic pressure obtained at a receiver at $x = 100\,\mathrm{m}$, $y = 0\,\mathrm{m}$, and $z = 2\,\mathrm{m}$ (a) for a downward-refracting and (b) an upward-refracting atmosphere using impedance models and parameters values (see Table II) giving best fits to short range data obtained over lawn, NORDTEST #30: (solid line) variable porosity and (dashed-dotted line) modified Miki impedance models.

value of the pressure is predicted to be somewhat less (about 67 instead of 82 Pa) when using the variable porosity model rather than the modified Miki model. In addition, the predicted low-frequency tails observable for $t > 0.291$ s are remarkably different. For an upward refracting atmosphere in Fig. 9(b), the signal has mainly a low-frequency content and, in accordance with the previous statements, the times series of the pressure are seen to significantly differ. For lawn, the time-domain predictions using the variable porosity and the modified Miki model are in a closer agreement. In particular, this is observed in Fig. 10(b) for an upward-refracting atmosphere. However, for a downward-refracting atmosphere in Fig. 10(a), the peak values of the acoustic pressure are again noticeably different, as the predicted maximum amplitude is 80 Pa using the variable porosity model but is only 60 Pa using the modified Miki model.

V. CONCLUDING REMARKS

It has been demonstrated that, in common with the single-parameter semi-empirical Delany and Bazley model on which they are based, three-parameter and modified Miki models result in predictions of negative values of the real part of complex effective density for small values of frequency divided by flow resistivity when considering ranges of frequency and flow resistivity of interest to outdoor sound predictions. This means that they are unsuitable for representing outdoor ground surfaces particularly if they are externally reacting. On the other hand, square root models (including phenomenological and Hamet models)[10] and a two-parameter slit pore impedance model do not lead to non-physical predictions. Also it has been shown that the slit pore impedance model for semi-infinite or finite hard-backed layer impedance satisfies all requirements for physical admissibility.

In addition it has been further demonstrated that use of the Miki-based models does not enable as good fits of data for short range propagation as do (a) the two-parameter variable porosity model over grassland and (b) the two-parameter slit pore model and its three-parameter hard-backed layer version over forest floors and gravel.

Use of semi-empirical impedance models such as those of Delany and Bazley and Miki for representing outdoor ground impedance has been popular since (i) either only a single parameter is required or two if hard-backed layer versions are used and (ii) they give tolerable agreement with data obtained over grassland and soils. However, there are three considerations that make the use of these semi-empirical models inadvisable when making outdoor sound predictions. First, these models are physically inadmissible. Second, they do not yield as good fits to short range ground characterisation data as alternative physically admissible models even when such models use only two parameters. For grassland the variable porosity model enables better fits. For low flow resistivity surfaces such as forest floors and gravel, slit pore layer models yield better fits. The three-parameter form of the Miki model enables similar agreement over low flow resistivity surfaces to that obtained by using physically admissible models such as the slit pore model. However, it should be noted that, in a study of the acoustical properties of green roofs (vegetation plus soil substrates), data fitting using the three-parameter Miki model was found to require non-physical values of the parameters (porosity greater than 1 and tortuosity less than 1).[25] Third, the fact that short range level difference magnitude data can be fitted by using significantly difference impedance spectra means that use of the semi-empirical single-parameter impedance models leads to substantial differences in frequency- and time-domain predictions at 100 and 500 m range compared with those obtained by using physically admissible ground impedance models. The differences between excess attenuation predictions at 500 m range associated with use of physically admissible impedance models instead semi-empirical physically inadmissible models are greater than those predicted due to the observed spatial variations at two grassland sites and comparable with those predicted at these sites due to observed seasonal differences.

The widespread use of semi-empirical impedance model with parameter values deduced from short range level difference magnitude fits rather than fits to the same data using alternative physically admissible two-parameter models to represent ground impedance adds an avoidable uncertainty to long range outdoor sound predictions. The standards and prediction schemes mentioned in the Introduction that recommend the Delany and Bazley model as a default choice should include a cautionary acknowledgement of the drawbacks of this model for representing outdoor ground impedance and should encourage either use of complex level difference spectra for direct model-independent deduction of ground impedance or other, preferably physically admissible, models including the two-parameter version of the slit pore model which has hitherto not featured in any standard or prediction scheme.

As a final comment we note that in specifying twelve and seven, respectively, effective flow resistivity classes NORDTEST ACOU 104 (Ref. 4) and the HARMONOISE report[5] imply that the Delany and Bazley model can be used for all ground surfaces. While it is acknowledged in the HARMONOISE report[5] that a different model (the Hamet model[9]) should be used for layered surfaces including porous asphalt, the results obtained in Ref. 7 and in this paper emphasize the fact that single impedance model should not expected to provide adequate representation of the acoustical properties of all ground surfaces.

ACKNOWLEDGMENTS

This work was granted access to the HPC resources of IDRIS under the allocation 2015-022203 made by GENCI (Grand Equipement National de Calcul Intensif). It was performed within the framework of the Labex CeLyA of Université de Lyon, operated by the French National Research Agency (Grant No. ANR-10-LABX-0060/ANR-11-IDEX-0007).

APPENDIX A: PROPERTIES OF THE FUNCTIONS $\tanh(z)$ AND $F(z) = \tanh(z)/z$

Some properties of the function $F(z) = \tanh(z)/z$ are demonstrated in this appendix. First, it is shown that

$$\text{for Arg}(z) \in \left[0; \frac{\pi}{4}\right], \quad \text{Im}\left[\frac{\tanh(z)}{z}\right] \leq 0, \tag{A1a}$$

$$\text{for Arg}(z) \in \left[-\frac{\pi}{4}; 0\right], \quad \text{Im}\left[\frac{\tanh(z)}{z}\right] \geq 0. \tag{A1b}$$

With this aim, by noting that the function tanh can be written for a complex number $z = x + iy$ as[17]

$$\tanh(z) = \frac{\sinh(2x) + i\sin(2y)}{\cosh(2x) + \cos(2y)}, \tag{A2}$$

one has

$$\frac{\tanh(z)}{z} = \frac{1}{x + iy}\frac{\sinh(2x) + i\sin(2y)}{\cosh(2x) + \cos(2y)}. \tag{A3}$$

The imaginary part of the function $\tanh(z)/z$ is thus given by

$$\text{Im}\left[\frac{\tanh(z)}{z}\right] = \frac{1}{|z|^2}\frac{x\sin(2y) - y\sinh(2x)}{\cosh(2x) + \cos(2y)}. \tag{A4}$$

In the first quadrant of the complex plane ($x \geq 0$ and $y \geq 0$), $\sin(y) \leq y$ and $x \leq \sinh(x)$, which yields Eq. (A1a). Similarly, in the fourth quadrant ($x \geq 0$ and $-y \geq 0$), $\sin(-y) \leq -y$ and $x \leq \sinh(x)$, which yields Eq. (A1b).

Then, it is shown that

$$\text{for Arg}(z) \in \left[-\frac{\pi}{4}; \frac{\pi}{4}\right], \quad \text{Re}\left[\frac{\tanh(z)}{z}\right] \geq 0. \tag{A5}$$

For that, the real part of the function $\tanh(z)/z$ is given from Eq. (A3) by

$$\text{Re}\left[\frac{\tanh(z)}{z}\right] = \frac{1}{|z|^2}\frac{x\sinh(2x) + y\sin(2y)}{\cosh(2x) + \cos(2y)}. \tag{A6}$$

Introducing $z = Re^{i\theta}$, this yields

$$\text{Re}\left[\frac{\tanh(z)}{z}\right] = \frac{1}{R}\frac{\cos\theta\sinh(2R\cos\theta) + \sin\theta\sin(2R\sin\theta)}{\cosh(2R\cos\theta) + \cos(2R\sin\theta)}. \tag{A7}$$

For $\theta \in [0;\pi/4]$, one has $\sin(2R\sin\theta) \geq -2R\sin\theta$ and $\sinh(2R\cos\theta) \geq 2R\cos\theta$. As $\cos\theta$ and $\sin\theta$ are positive, one obtains the inequality

$$\cos\theta\sinh(2R\cos\theta) + \sin\theta\sin(2R\sin\theta) \geq 2R(\cos^2\theta - \sin^2\theta) \geq 0, \tag{A8}$$

which shows that $\text{Re}[\tanh(z)/z] \geq 0$. A similar inequality is also obtained for $\theta \in [-\pi/4;0]$, which demonstrate Eq. (A5).

In addition, one has also the property

$$\text{for Arg}(z) \in \left[-\frac{\pi}{4}; \frac{\pi}{4}\right], \quad \left|\frac{\tanh(z)}{z}\right| \leq 1. \tag{A9}$$

Using the relation[17]

$$|\tanh(x + iy)| = \left(\frac{\cosh(2x) - \cos(2y)}{\cosh(2x) + \cos(2y)}\right)^{1/2}, \tag{A10}$$

the modulus of tanh can be obtained through

$$|\tanh(Re^{i\theta})| = \left(\frac{\cosh(2R\cos\theta) - \cos(2R\sin\theta)}{\cosh(2R\cos\theta) + \cos(2R\sin\theta)}\right)^{1/2}. \tag{A11}$$

The inequality in Eq. (A9) is therefore equivalent to

$$\frac{\cosh(2R\cos\theta) - \cos(2R\sin\theta)}{R^2} \leq \cosh(2R\cos\theta) + \cos(2R\sin\theta), \tag{A12}$$

which can be demonstrated by checking the coefficients of each term in the Maclaurin series of both functions. In details, by noting $f(R) = (\cosh(2R\cos\theta) - \cos(2R\sin\theta))/R^2$ and $g(R) = \cosh(2R\cos\theta) + \cos(2R\sin\theta)$, one has

$$f(R) = \sum_{n=0}^{\infty} a_n R^{2n}, \text{ with } a_n = 2^{2n+2}\frac{\cos^{2n+2}\theta + (-1)^n\sin^{2n+2}\theta}{(2n+2)!}, \tag{A13a}$$

$$g(R) = \sum_{n=0}^{\infty} b_n R^{2n}, \text{ with } b_n = 2^{2n}\frac{\cos^{2n}\theta + (-1)^n\sin^{2n}\theta}{(2n)!}. \tag{A13b}$$

For $\theta \in [-\pi/4, \pi/4]$, it is straightforwardly checked that $0 \leq a_n \leq b_n$, which yields that $f(R) \leq g(R)$ and gives finally Eq. (A9).

It is also shown that

$$F(z) \text{ tends uniformly to 0 as } |z| \to \infty \text{ in } -\frac{\pi}{4} \leq \text{Arg}(z) \leq \frac{\pi}{4}. \tag{A14}$$

For that, a first upper bound of $F(z)$ is obtained using Eq. (A11),

$$|F(z)| \leq \frac{1}{R}\left(\frac{\cosh(2R\cos\theta) + 1}{\cosh(2R\cos\theta) - 1}\right)^{1/2}. \tag{A15}$$

The function in this inequality is decreasing with $\cos\theta$ and, hence, its maximum is obtained for $\theta = \pm\pi/4$. This leads to

$$|F(z)| \leq \frac{1}{R}\left(\frac{\cosh(\sqrt{2}R) + 1}{\cosh(\sqrt{2}R) - 1}\right)^{1/2}, \tag{A16}$$

which shows that $F(z)$ tends uniformly to 0 in $\text{Arg}(z) \in [-\pi/4, \pi/4]$ as $R \to \infty$.

Finally, it is demonstrated that

$$\tanh(z) \text{ tends uniformly to 1 as } |z| \to \infty \text{ in } -\frac{\pi}{4} \le \mathrm{Arg}(z) \le \frac{\pi}{4}. \tag{A17}$$

Indeed, from Eq. (A2), one has

$$\begin{aligned}|\tanh(z) - 1|^2 &= \frac{\left(e^{-2R\cos\theta} - \cos(2R\sin\theta)\right)^2 + \sin^2(2R\sin\theta)}{\left(\cosh(2R\cos\theta) + \cos(2R\sin\theta)\right)^2} \\ &\le \frac{3}{\left(\cosh(2R\cos\theta) - 1\right)^2} \\ &\le \frac{3}{\left(\cosh(\sqrt{2}R) - 1\right)^2},\end{aligned}$$

which shows that $\tanh(z)$ is converging exponentially and uniformly to 1 in $\mathrm{Arg}(z) \in [-\pi/4, \pi/4]$ as $R \to \infty$.

APPENDIX B: APPLICATION TO F_1 AND F_2

In this appendix, the relations obtained in Appendix A are used to obtain some properties of the functions $f_1(z)$ and $f_2(z)$ defined in Eqs. (15) in $\mathrm{Arg}(z) \in [-\pi/4, \pi/4]$.

First, the zeros of these functions are investigated. As Eq. (A5) implies $\mathrm{Re}[f_2] \ge 1$, it is concluded that f_2 has no zeroes in this region of the complex plane. Note that $f_1(z=0)=0$. For $z=x+iy \ne 0$, $f_1(z)=0$ implies that $\mathrm{Im}[\tanh z/z] = 0$, which yields from Eq. (A4),

$$\left|\frac{\sinh(2x)}{2x}\right| = \left|\frac{\sin(2y)}{2y}\right|. \tag{B1}$$

As $|\sinh(2x)| \ge |2x|$ and $|\sin(2y)| \le |2y|$, this equality is possible only when $|\sinh(2x)| = |2x|$ and $|\sin(2y)| = |2y|$, which implies $x=0$ and $|\sin(2y)| = |2y|$. Therefore, in $\mathrm{Arg}(z) \in [-\pi/4; \pi/4]$, the only zero of f_1 is 0.

From Eqs. (A5) and (A9), it is deduced that

$$\text{For } \mathrm{Arg}(z) \in \left[-\frac{\pi}{4}; \frac{\pi}{4}\right], \quad \mathrm{Re}[f_1](z) \ge 0 \text{ and } \mathrm{Re}[f_2](z) \ge 0. \tag{B2}$$

Moreover, Eqs. (A1) lead to

$$\text{For } \mathrm{Arg}(z) \in \left[-\frac{\pi}{4}; 0\right], \quad \mathrm{Im}[f_1] \le 0 \text{ and } \mathrm{Im}[f_2] \ge 0, \tag{B3a}$$

$$\text{For } \mathrm{Arg}(z) \in \left[0; \frac{\pi}{4}\right], \quad \mathrm{Im}[f_1] \ge 0 \text{ and } \mathrm{Im}[f_2] \le 0. \tag{B3b}$$

Finally, it is concluded that

$$\text{For } \mathrm{Arg}(z) \in \left[-\frac{\pi}{4}; 0\right], \quad -\frac{\pi}{2} \le \mathrm{Arg}[f_1] \le 0 \text{ and } 0 \le \mathrm{Arg}[f_2] \le \frac{\pi}{2}, \tag{B4a}$$

$$\text{For } \mathrm{Arg}(z) \in \left[0, \frac{\pi}{4}\right], \quad 0 \le \mathrm{Arg}[f_1] \le \frac{\pi}{2} \text{ and } -\frac{\pi}{2} \le \mathrm{Arg}[f_2] \le 0. \tag{B4b}$$

[1] M. Delany and E. Bazley, "Acoustical properties of fibrous absorbent materials," Appl. Acoust. **3**, 105–116 (1970).
[2] Y. Miki, "Acoustical properties of porous materials—Modifications of Delany-Bazley models," J. Acoust. Soc. Jpn. **11**(1), 19–24 (1990).
[3] ANSI/ASA S1.18-2010: *American National Standard Method for Determining the Acoustic Impedance of Ground Surfaces* (Acoustical Society of America, New York, 2010).
[4] NORDTEST ACOU 104: *Ground Surfaces: Determination of Acoustic Impedance* (1998), http://www.nordtest.info/index.php/methods/item/ground-surfaces-determination-of-the-acoustic-impedance-nt-acou-104.html (Last viewed 05/21/15).
[5] R. Nota, R. Barelds, D. van Maercke, and J. J. A. van Leeuwen, HARMONOISE WP 3, "Engineering method for road traffic and railway noise after validation and fine-tuning," Technical Report No. HAR32TR-040922-DGMR20 (2005).
[6] European Noise Directive 2002/49/EC of the European Parliament and of the Council.
[7] K. Attenborough, I. Bashir, and S. Taherzadeh, "Outdoor ground impedance models," J. Acoust. Soc. Am. **129**(5), 2806–2819 (2011).
[8] D. K. Wilson, "Simple relaxational models for the acoustical properties of porous media," Appl. Acoust. **50**, 171–188 (1997).
[9] M. Bérengier, M. R. Stinson, G. A. Daigle, and J. F. Hamet, "Porous road pavement: Acoustical characterization and propagation effects," J. Acoust. Soc. Am. **101**(1), 155–162 (1997).
[10] D. Dragna and P. Blanc-Benon, "Physically admissible impedance models for time-domain computations of outdoor sound propagation," Acta Acust. Acust. **100**(3), 401–410 (2014).
[11] Y. Miki, "Acoustical properties of porous materials—Generalizations of empirical models," J. Acoust. Soc. Jpn. **11**, 25–28 (1990).
[12] G. Guillaume, F. Faure, B. Gauvreau, F. Junker, and M. Bérengier, "Estimation of impedance model input parameter from *in situ* measurements: Principles and applications," Appl. Acoust. **95**, 27–36 (2015).
[13] S. W. Rienstra, "Impedance models in time domain including the Helmholtz resonator model," in *Twelfth AIAA/CEAS Aeroacoustics Conference*, Cambridge, MA, 2006, AIAA Paper 2006–2686.
[14] E. Salomons, *Computational Atmospheric Acoustics* (Kluwer, Dordrecht, 2001), p. 118.
[15] K. Horoshenkov, A. Khan, and H. Benkreira, "Acoustic properties of low growing plants," J. Acoust. Soc. Am. **133**(5), 2554–2565 (2013).
[16] R. Kirby, "On the modification of Delany and Bazley fomulae," Appl. Acoust. **86**, 47–49 (2014).
[17] M. Abramowitz and I. Stegun, *Handbook of Mathematical Functions* (Dover, New York, 1965), p. 70, formula 4.2.39; p. 84, formula 4.5.51; p. 1022, formulas 29.3.7 and 29.3.11; p. 1023, formula 29.3.40; p. 1026, formula 29.3.82.
[18] Available from the authors. See also M. Ögren and H. Jonasson, "Measurement of the Acoustic Impedance of the Ground," SP Swedish National Testing and Research Institute, Report No. 1998:28.
[19] H. Taraldsen and G. Jonasson, "Aspects of ground effect modeling," J. Acoust. Soc. Am. **129**(1), 47–53 (2011).
[20] K. Attenborough, K. M. Li, and K. Horoshenkov, *Predicting Outdoor Sound* (Taylor and Francis, London, 2007), pp. 329, 330.
[21] D. Dragna, P. Blanc-Benon, and F. Poisson, "Time-domain solver in curvilinear coordinates for outdoor sound propagation over complex terrain," J. Acoust. Soc. Am. **133**(6), 3751–3763 (2013).
[22] D. Dragna, P. Pineau, and P. Blanc-Benon, "A generalized recursive convolution method for time-domain propagation in porous media," J. Acoust. Soc. Am. **138**(2), 1030–1042 (2015).
[23] C. Bogey and C. Bailly, "A family of low dispersive and low dissipative explicit schemes for flow and noise computations," J. Comput. Phys. **194**, 194–214 (2004).
[24] B. Cotté, P. Blanc-Benon, C. Bogey, and F. Poisson, "Time-domain impedance boundary conditions for simulations of outdoor sound propagation," AIAA J. **47**(10), 2391–2403 (2009).
[25] C. Liu and M. Hornikx, "Determination of the impedance of vegetated roofs with a double-layer Miki model," *Proceedings of Euronoise 2015*, NAG, Maastricht.